

# Majorana Fermions and Multiple Topological Phase Transition in Kitaev Ladder Topological Superconductors

Ryohei Wakatsuki<sup>1</sup>, Motohiko Ezawa<sup>1</sup> and Naoto Nagaosa<sup>1,2</sup>

<sup>1</sup>*Department of Applied Physics, University of Tokyo, Hongo 7-3-1, 113-8656, Japan and*

<sup>2</sup>*Center for Emergent Matter Science (CEMS), ASI, RIKEN, Wako 351-0198, Japan*

Motivated by the InSb nanowire superconductor system, we investigate the system where one-dimensional topological superconductors are placed in parallel. It would well be simulated by a ladder of the Kitaev chains. The system undergoes multiple topological phase transitions, where the number of Majorana fermion changes as a function of the inter-chain superconducting pairings. We analytically determine the topological phase diagram by explicitly calculating the topological number and the band structure. They show the even-odd effects with respect to the number of legs of the ladder. When the relative phase between the inter- and intra-chain superconducting pairings is zero or  $\pi$ , the system belongs to the class BDI with the  $\mathbb{Z}$  index, and otherwise it belongs to the class D with the  $\mathbb{Z}_2$  index. This topological class change would be caused by applying the Josephson current or external magnetic field, and could be observed by measuring the Andreev reflection and crossed Andreev reflection rates.

## I. INTRODUCTION

Majorana fermion is one of the hottest topics in the condensed matter physics<sup>1,2</sup>. Majorana fermions are particles which are their own antiparticles. Because of their non-locality and non-Abelian statistics, they are considered to realize exotic phenomena and there are possibilities to encode fault tolerant topological quantum computations. There are several suggestions for physical systems that support Majorana zero-energy states (MZES). The Kitaev model is the simplest model that realizes the MZES<sup>6</sup>. For example, it well describes the helical edge states of the two-dimensional topological insulator with superconducting proximity effects<sup>3</sup> and one-dimensional nanowire with strong spin-orbit interaction<sup>4,5</sup>. There are generalizations of the Kitaev model by several authors<sup>7-14</sup>.

Epitaxially grown InSb nanowires are the most promising material systems for the formation of a hybrid device with an *s*-wave superconductor in which the excitation of Majorana fermions can be achieved under an application of an external magnetic field of a moderate strength<sup>4,5</sup>. InSb nanowires possess a large electron *g* factor ( $|g| \sim 50$ ), a strong spin-orbit interaction (SOI) strength (with the SOI energy in the order of  $\Delta_{\text{SOI}} = 0.3$  meV), and a small electron effective mass ( $m^* = 0.015m_e$ ). These properties allow us to generate a helical liquid in the InSb nanowire by applying a relatively small magnetic field and to generate a nontrivial topological superconductor, which supports a pair of Majorana fermions, by coupling the InSb nanowire to an *s*-wave superconductor in an experimentally feasible condition. The *s*-wave superconductor will introduce superconductivity into the InSb nanowire by proximity effect and the external magnetic field will then drive the strongly spin-orbit coupled nanowire system into a nontrivial topological superconductor phase through the Zeeman splitting. Recently, the signature of zero energy bound states was observed in the system using InSb or

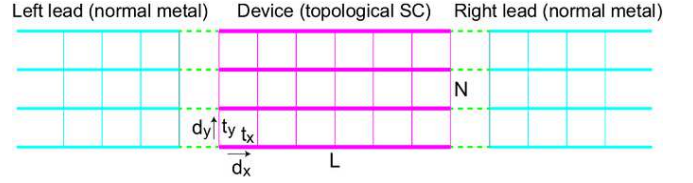


FIG. 1: (Color online) Illustration of a ladder topological superconductor. It is decomposed into the device, right lead and left lead parts. The red region is a device of the ladder topological superconductor. Heavy lines indicate the chains, while the narrow lines indicate the inter-chain couplings.  $L$  is the number of sites along the chains, while  $N$  is the number of the chains. The blue regions are right and left leads.

InAs nanowire<sup>15-18</sup>.

In this paper, motivated by the InSb nanowire system, we investigate the system where one-dimensional topological superconductors are placed in parallel. The system would well be simulated by the ladder of topological superconductors shown in Fig.1. We first analyze the system where the inter-chain superconducting coupling is absent. The system belongs to the class BDI, where the topological number is characterized by the  $\mathbb{Z}$  index. We find that the number of the MZES changes from  $N$  to 0 by changing the magnitude of the interlayer hopping. We determine the topological phase diagram by calculating the  $\mathbb{Z}$  index, which is a topological number of the system. Next we introduce the inter-chain superconducting pairings. When the relative phase between the inter- and intra-superconducting pairings is 0 or  $\pi$ , the system belongs to the class BDI and is characterized by the  $\mathbb{Z}$  index. On the other hand, otherwise, the system turns into the class D and is characterized by the  $\mathbb{Z}_2$  index: The number of the MZES changes alternately between 0 and 1 due to the repulsion by the inter-chain superconducting pairings.

The rest of the paper is organized as follows. In Sec.II we introduce the model and discuss the relationship be-

tween our model and the Kitaev model. We also discuss the symmetry and the topological classification of the Hamiltonian. In Sec.III and IV, we study the model without and with inter-chain superconducting pairing. We calculate the  $\mathbb{Z}$  and  $\mathbb{Z}_2$  indices and determine the phase diagram. We also discuss the energy spectrum with and without the inter-chain superconducting pairings. In Sec.V we derive the low-energy effective Hamiltonian written in terms of Majorana operators and discuss its low energy behavior. In Sec.VI, examining the transport property of the model, we study how the conductance depends on the phase difference between intra- and inter-chain superconducting pairings.

## II. KITAEV LADDER MODEL

Majorana fermions emerge at the edges of an InSb nanowire in the presence of the superconducting order and the external magnetic field perpendicular to it. It is well described by the Kitaev chain<sup>6</sup>, where a one-dimensional  $p$ -wave topological superconductivity is realized. A natural question is what happens when we place several InSb nanowires in parallel. This set-up will be easily realized by a recent nanofabrication technology.

To simulate this system, we propose to investigate the Hamiltonian describing a ladder of the Kitaev chains,

$$\begin{aligned}
H = & -\mu \sum_{i,j} c_{i,j}^\dagger c_{i,j} \\
& - \sum_{i,j} (t_x c_{i,j}^\dagger c_{i+1,j} + t_y c_{i,j}^\dagger c_{i,j+1} + \text{h.c.}) \\
& - \sum_{i,j} (d_x c_{i,j}^\dagger c_{i+1,j}^\dagger + d_y c_{i,j}^\dagger c_{i,j+1}^\dagger + \text{h.c.}), \quad (1)
\end{aligned}$$

where  $i$  and  $j$  are the lattice coordinates for the  $x$  and  $y$  axes. The intra-chain transfer integral  $t_x$  and the intra-chain superconducting pairing amplitude  $d_x$  are present in the Kitaev model, while we newly obtain the effective inter-chain transfer integral  $t_y$  and the superconducting pairing amplitude  $d_y$ .

There is an important comment on the coefficients  $d_x$  and  $d_y$ . By making a phase transformation of  $c_{i,j}$ , we can change the overall phase of the superconducting pairings. Namely, the phase difference between  $d_x$  and  $d_y$  is physical, but the absolute phases of  $d_x$  and  $d_y$  are meaningless. Without loss of generality we may assume that  $d_x$  is real in the effective Hamiltonian, while  $d_y$  is complex in general. We define  $\theta$  as the phase of  $d_y$ , i.e.,  $d_y = |d_y|e^{i\theta}$ .

The energy spectrum is symmetric around the zero energy due to the particle-hole symmetry induced by the superconductivity. There are  $N$  legs in the ladder [Fig.1]. We refer to  $L$  as the number of sites along the ladder. We note that the system is reduced to the Kitaev chain when  $N = 1$ . If the phase difference between  $d_x$  and  $d_y$  is  $\pi/2$  and  $L \approx N$  it is anisotropic  $p + ip$  superconductor system. We analyze mainly small  $N$  region.

We clarify the topological class<sup>19</sup> of the Hamiltonian (1). In the momentum representation, the Bogoliubov de Gennes Hamiltonian is given by

$$H_{BdG}(k) = \begin{pmatrix} \xi & \Delta \\ \Delta^\dagger & -\xi \end{pmatrix}, \quad (2)$$

where  $\xi$  and  $\Delta$  are  $N \times N$  tridiagonal matrices with the matrix elements

$$\xi_{i,j} = (-\mu - 2t_x \cos k) \delta_{i,j} - t_y \delta_{i,j+1} - t_y \delta_{i+1,j}, \quad (3)$$

$$\Delta_{i,j} = 2id_x \sin k \delta_{i,j} + d_y \delta_{i,j+1} - d_y \delta_{i+1,j}, \quad (4)$$

where  $k$  is the crystal momentum along the chain direction, i.e., the  $x$  axis.

The explicit representation of the time reversal ( $\Theta$ ), the particle-hole reversal ( $\Xi$ ) and the chiral ( $\Pi$ ) operator are defined by

$$\Theta = K, \quad \Xi = \tau_x K, \quad \Pi = \tau_x, \quad (5)$$

where  $K$  represents the complex conjugate operator. We can show the Hamiltonian satisfies the relation

$$\Xi^\dagger H(-k) \Xi = -H(k), \quad (6)$$

$$\Pi^\dagger H(-k) \Pi = -H(k). \quad (7)$$

When  $\text{Im}d_y = 0$ , the Hamiltonian satisfies the relation

$$\Theta^\dagger H(-k) \Theta = H(k). \quad (8)$$

It is easily seen that  $\Theta^2 = \Pi^2 = \Xi^2 = 1$ . Then, the Hamiltonian belongs to the class BDI, which is characterized by the  $\mathbb{Z}$  index. On the other hand, when  $\text{Im}d_y \neq 0$ , the time-reversal symmetry is broken, and the class changes to the class D where only  $\Xi$ -symmetry is there, being characterized by the  $\mathbb{Z}_2$  index.

It is convenient to use the Majorana representation, which is constructed with use of the unitary transformation,

$$U = \frac{1}{\sqrt{2}} \begin{pmatrix} \mathbb{I} & i\mathbb{I} \\ \mathbb{I} & -i\mathbb{I} \end{pmatrix}, \quad (9)$$

where  $\mathbb{I}$  is the unit matrix. It transforms Dirac fermions into Majorana fermions,

$$c_{i,j}^\dagger = \frac{\gamma_{i,j}^A + i\gamma_{i,j}^B}{2}, \quad c_{i,j} = \frac{\gamma_{i,j}^A - i\gamma_{i,j}^B}{2}, \quad (10)$$

obeying  $\{\gamma_{i,j}, \gamma_{i',j'}\} = \delta_{i,i'} \delta_{j,j'}$ . The unitary transformed Hamiltonian is given by

$$U^\dagger H U = \frac{1}{2} \begin{pmatrix} \Delta + \Delta^\dagger & 2i\xi - i(\Delta - \Delta^\dagger) \\ -2i\xi - i(\Delta - \Delta^\dagger) & -(\Delta + \Delta^\dagger) \end{pmatrix}. \quad (11)$$

Our analysis is carried on based on this Majorana representation of the Hamiltonian.

### III. TOPOLOGICAL PHASE DIAGRAM WITHOUT INTER-CHAIN SUPERCONDUCTING PAIRINGS

We first investigate the case of  $d_y = 0$  for simplicity. The transformed Hamiltonian is written as

$$U^\dagger H U = i \begin{pmatrix} 0 & v \\ -v^T & 0 \end{pmatrix}, \quad (12)$$

which has only off-diagonal elements, with

$$\begin{aligned} v &= \xi - \frac{1}{2}(\Delta - \Delta^\dagger) \\ &= (-\mu - 2t_x \cos k - 2id_x \sin k) \mathbb{I} - t_y \mathbb{M}, \end{aligned} \quad (13)$$

where  $\mathbb{M}$  represents a tridiagonal matrix which only has elements 1 at  $(n, n+1)$  and  $(n+1, n)$ . It is straightforward to diagonalize the matrix  $v$ . As we see at the end of this section, the eigenvalues are

$$z_n = -\mu - 2t_y \cos \frac{n}{N+1}\pi - 2t_x \cos k - 2id_x \sin k, \quad (14)$$

while the eigenfunctions are

$$\Psi_n = \sqrt{\frac{2}{N+1}} \sin \frac{n}{N+1}\pi m \quad (n = 1, 2, \dots, N), \quad (15)$$

where  $m$  represents the position ( $m = 1, 2, \dots, N$ ).

The chiral index  $W$  is defined by

$$W \equiv \text{tr} \int \frac{dk}{2\pi i} \partial_k \log v(k) = \sum_n \int \frac{dk}{2\pi i} \partial_k \log z_n(k), \quad (16)$$

where  $z_n$  are the eigenvalues of  $v$ . It describes the sum of the winding numbers of  $v(k)$  around the origin of the complex plane. The chiral index is calculable by substituting (14) into (16).

We investigate the topological phase diagram in the  $(t_y, \mu)$  plane. The phase boundaries are determined by  $\det v = 0$ . It follows from (14) that they are given by

$$-\mu - 2t_y \cos \frac{n}{N+1}\pi = \pm 2t_x. \quad (17)$$

The topological phase diagram is illustrated in Fig.2. We see the following characteristic features: The chiral index is  $W = N$  at  $(t_y, \mu) = (0, 0)$ . Along the  $\mu$  axis with  $t_y = 0$ , the topological phase transition occurs from  $W = N$  to  $W = 0$  at  $\mu = \pm 2t_x$  irrespective of the number  $N$  of the legs. On the other hand, along the  $t_y$  axis with  $\mu = 0$ , multiple topological phase transitions occur: The band gap closes at  $t_y = \pm \frac{2t_x}{z_n}$ , and the chiral index is 0 for even  $N$  and 1 for odd  $N$  for sufficiently large  $t_y$ .

We show the energy spectrum of the ladder of chains as a function of  $t_y$  for  $N = 4, 5$  in Fig.3. We find that the chiral index gives the number of MZES. The wave functions of all the MZES are localized at the edges.

The above behaviors can be understood as follows. The system is equivalent to the  $N$  independent Kitaev

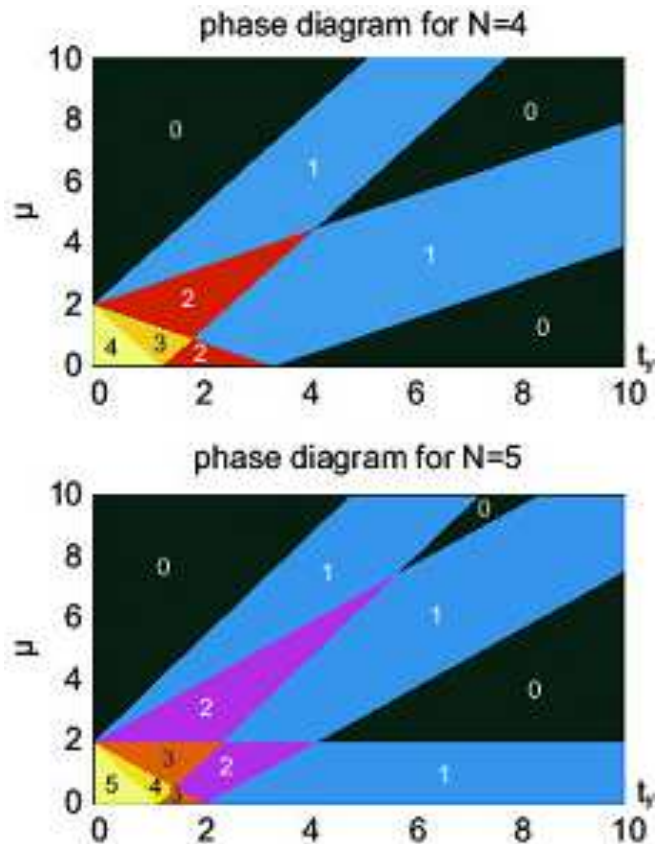


FIG. 2: (Color online) Phase diagrams of the four-leg and five-leg ladder. We have taken  $t_x = 1.0, d_x = 0.5, d_y = 0$ . The system is described by the  $\mathbb{Z}$  index, with the number in the figure representing the chiral index  $W$ .

chains with the renormalized chemical potential  $\mu' = \mu + 2t_y \cos \frac{n}{N+1}\pi$ . Each renormalized Kitaev chain has MZES when  $|\mu'| < 2|t_x|$ . The total number of the MZES is given by the sum of the renormalized Kitaev chains.

For the sake of completeness we show how to derive the eigenvalues (14). The eigenvalues  $z_n$  can be obtained by solving the characteristic equation for  $t_y \mathbb{M}$  is

$$f_N(x) = \det(x\mathbb{I} - t_y \mathbb{M}) = 0. \quad (18)$$

To solve this we write down the recurrence relation of the characteristic equation,

$$f_{N+2}(x) = x f_{N+1}(x) - t_y^2 f_N(x), \quad (19)$$

from which it follows that

$$f_N(x) = t_y^N U_N \left( \frac{x}{2t_y} \right) = \sum_{n=0}^{[N/2]} (-1)^n \binom{N-n}{n} t_y^{2n} x^{N-2n} \quad (20)$$

with the Chebyshev polynomials of the second kind. We now solve the eigenequation as

$$x_n = 2t_y \cos \frac{n}{N+1}\pi \quad (n = 1, 2, \dots, N), \quad (21)$$

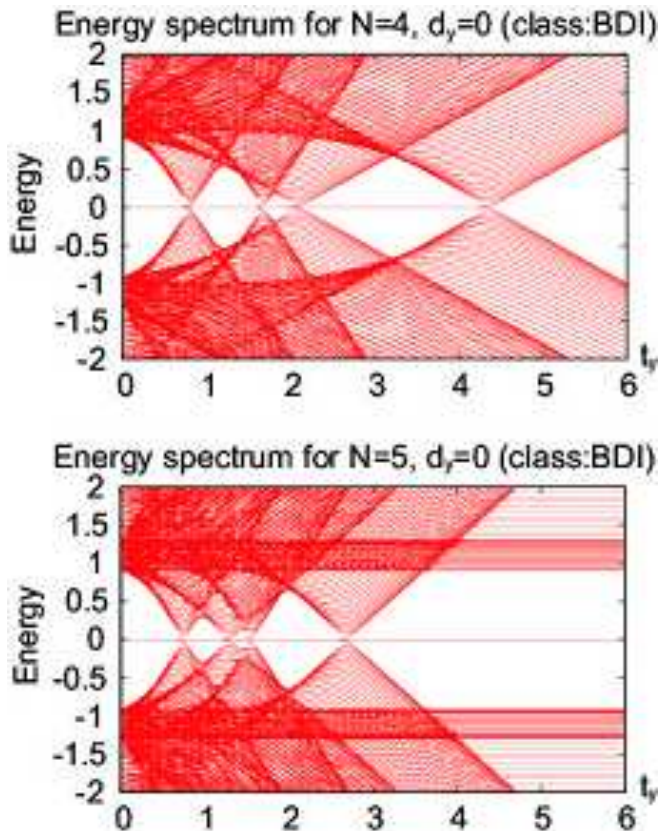


FIG. 3: (Color online) Energy spectra of  $N = 4, 5$  ladder with  $d_y = 0$ . We have taken  $\mu = 0.7, t_x = 1.0, d_x = 0.5$ . The number of zero energy states decreases by two at every phase transition as  $t_y$  increases, since each zero-energy state per chain doubly degenerates due to the two end points of the chain. In the strong coupling limit  $t_y \rightarrow \infty$ , there is no (one) MZES per each edge in case of  $N = 4(5)$ . We have set  $L = 100$ .

from which we find the eigenvalues (14) and the eigenfunctions (15) because  $z_n$  is constants minus  $x_n$ .

#### IV. TOPOLOGICAL PHASE DIAGRAM WITH INTER-CHAIN SUPERCONDUCTING PAIRINGS

We next investigate the case  $d_y \neq 0$ . We first assume that it is real as well as  $d_x$ . Then, the system belongs to the class BDI, and the system is characterized by the  $\mathbb{Z}$  index. Physically, the phase difference between superconducting pairings disappears, and the sub-gap states with finite energy recovers to be Majorana fermions. We show the energy spectrum in Fig.4.

We proceed to investigate the effects of complex inter-chain superconducting pairings ( $\text{Im}d_y \neq 0$ ). The Hamiltonian no longer satisfies the time-reversal symmetry (8). The topological class of the Hamiltonian changes to the class D, and the topological number is the  $\mathbb{Z}_2$  index. The system allows only the two cases, i.e., whether a pair of

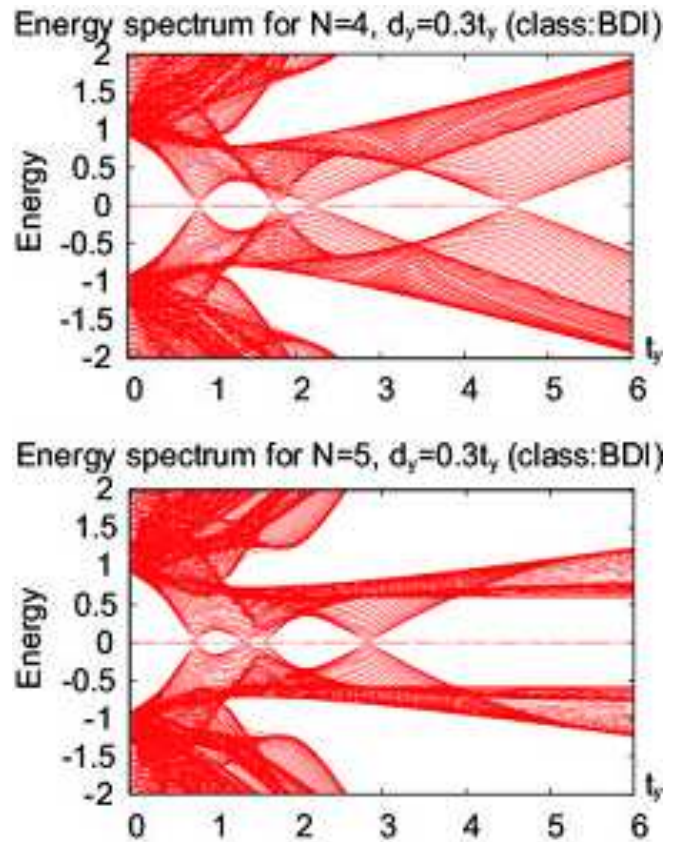


FIG. 4: (Color online) Energy spectra of  $N = 4, 5$  ladder with  $d_y = 0.3t_y$ . We have taken  $\mu = 0.7, t_x = 1.0, d_x = 0.5$ . Note that both  $d_x$  and  $d_y$  are real. The number of zero energy states decreases by two at every topological phase transition with the gap closing of the bulk states, because each zero energy states per chain doubly degenerates due to the two end points of the chain. In the strong coupling limit  $t_y \rightarrow \infty$ , there is no (one) MZES per each edge in case of  $N = 4(5)$ . We have set  $L = 100$ .

Majorana fermions exist or not.

We show the energy spectrum as a function of  $t_y$  in the presence of  $d_y$  [Fig.5]. The behavior of the MZES drastically changes from the system with  $d_y = 0$  to the one with  $\text{Im}d_y \neq 0$ . The MZES disappears in the region where the number of the MZES pairs is even. On the other hands, there is only one MZES pair in the region where the number of the MZES pairs is odd. This is due to the interference of MZES pairs due to the inter-chain superconducting pairings. Then, only one MZES pair can exist, which implies that the topological number is the  $\mathbb{Z}_2$  index. The number of MZES pairs is given by  $\text{mod}_2 N$ .

The  $\mathbb{Z}_2$  index is obtained by the sign of the Pfaffian at the time reversal invariant momenta  $k = 0$  and  $\pi$ . At these points, since  $d_x$  disappears from  $\Delta$  defined by (4), it is convenient to make a phase transformation  $c \mapsto e^{i\theta/2}c$ , so that  $d_y$  becomes real. Then, the Majorana represented

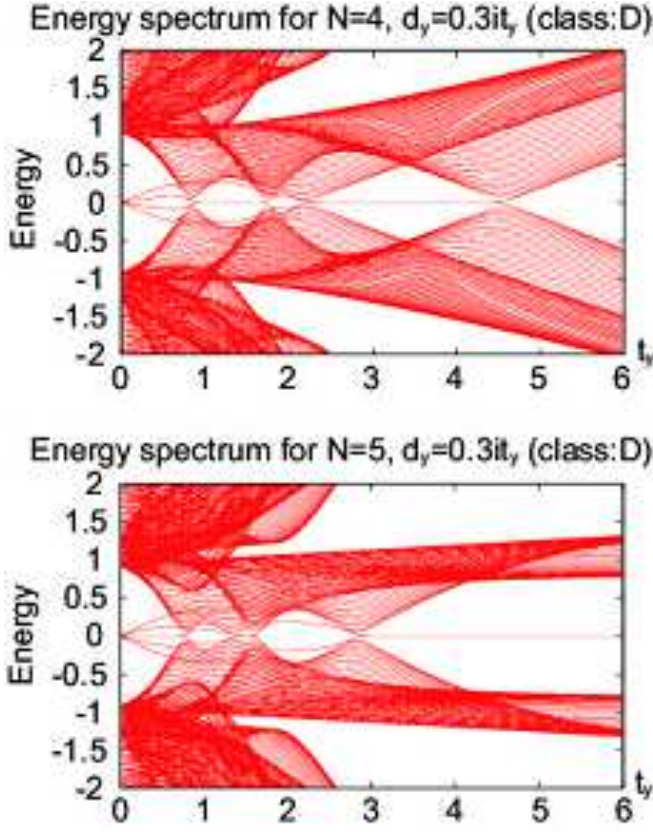


FIG. 5: (Color online) Energy spectra of  $N = 4, 5$  ladder with  $|d_y| < t_y$ . We have taken  $\mu = 0.7, t_x = 1.0, d_x = 0.5$  and  $d_y = 0.3it_y$ . Each sub-gap state doubly degenerates. With  $\text{Im}d_y \neq 0$ , MZES disappears in the parameter region where there are even MZES for  $d_y = 0$ , while two MZES remains in the parameter region where there are odd MZES for  $d_y = 0$ . In the strong coupling limit  $t_y \rightarrow \infty$ , there is no (one) MZES per each edge in case of  $N = 4(5)$ . We have set  $L = 100$ .

Hamiltonian at these points is given by (12), i.e.,

$$U^\dagger H U = i \begin{pmatrix} 0 & v \\ -v^T & 0 \end{pmatrix} \quad (22)$$

but now with

$$\begin{aligned} v &= (\xi_\pm - \Delta) \\ &= (-\mu \pm 2t_x) \delta_{i,j} - (t_y + |d_y|) \delta_{i,j+1} - (t_y - |d_y|) \delta_{i+1,j}, \end{aligned} \quad (23)$$

where  $\xi_- = \xi(0) = -\mu - 2t_x$  and  $\xi_+ = \xi(\pi) = -\mu + 2t_x$ .

The Pfaffian is simply given by

$$\text{Pf} \begin{pmatrix} 0 & v_\alpha \\ -v_\alpha^T & 0 \end{pmatrix} = \pm \det v_\alpha, \quad (24)$$

with  $\alpha = \pm$ , since there are no diagonal elements. The topological phase boundaries are determined by  $\det v = 0$  as before.

We obtain the recursion relation of the characteristic polynomial  $f_N = \det v$  as

$$f_{N+2} = (-\mu \pm 2t_x) f_{N+1} - (t_y^2 - |d_y|^2) f_N. \quad (25)$$

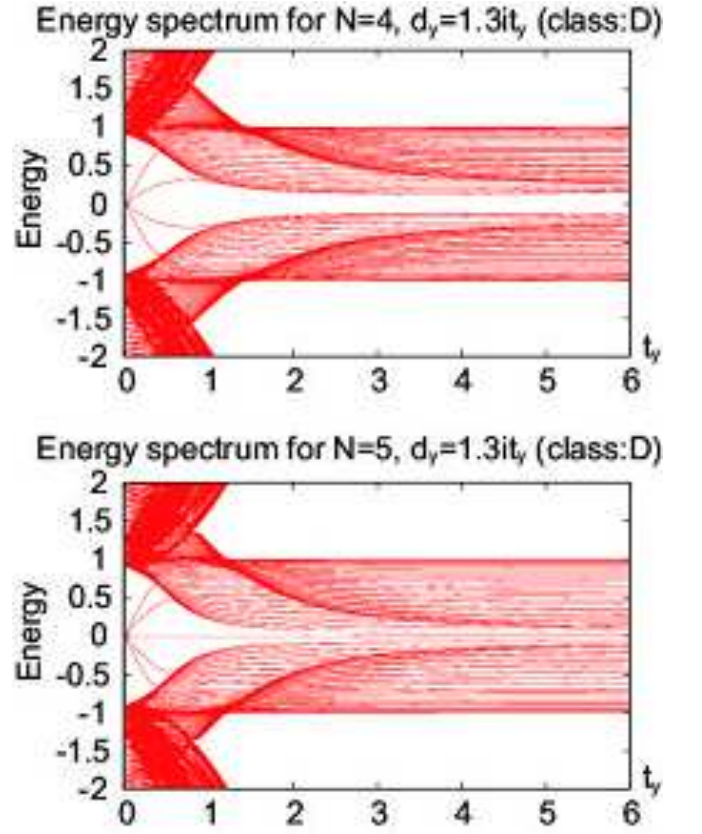


FIG. 6: (Color online) Energy spectra of  $N = 4, 5$  ladder with  $|d_y| > t_y$ . We have taken  $\mu = 0.7, t_x = 1.0, d_x = 0.5$  and  $d_y = 1.3it_y$ . Each sub-gap state doubly degenerates. When  $N = 4(5)$ , the system is always trivial (topological). We have set  $L = 100$ .

This relation is obtained by replacing  $t_y^2$  to  $t_y^2 - |d_y|^2$  in (19). Then, the condition  $f_N = 0$  yield

$$\mu - 2\sqrt{t_y^2 - |d_y|^2} \cos \frac{n}{N+1} \pi = \pm 2t_x, \quad (26)$$

which is nothing but (17) with the replacement of  $t$  by  $t'_y = \sqrt{t_y^2 - |d_y|^2}$ . The phase diagram depends on only  $|d_y|$ .

We obtain the phase diagram as follows. When  $|t_y| > |d_y|$ , it is simply given by Fig.2 with the understanding that the horizontal axis is  $t'_y$ . Recall that the energy spectrum as a function of  $t_y$  is given by Fig.5. On the other hand, when  $|d_y| > t_y$ ,  $t'_y$  becomes pure imaginary, and the phase diagram becomes very simple: When  $N$  is odd, the gap closing condition is given only by  $\mu = \pm 2t_x$ . When  $N$  is even, on the other hand, the system is trivial in the whole range. The energy spectrum as a function of  $t_y$  is now given by Fig.6.

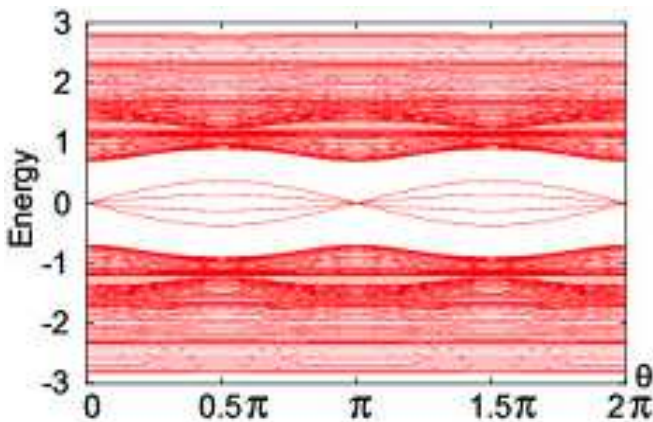


FIG. 7: (Color online) Energy spectrum as a function of the superconducting pairing phase  $\theta$ . There are four MZES in the case of  $N = 4$ , which are well described by the low-energy theory (29).

## V. ENERGY SPECTRUM AS A FUNCTION OF THE SUPERCONDUCTING PHASE DIFFERENCE

We show the energy spectrum as a function of  $\theta$  defined by  $d_y = |d_y|e^{i\theta}$  in Fig.7. It is clearly seen the MZES in the bulk band gap. We can construct the effective model which contains only Majorana states in the low energy region. First, we consider the case of  $d_y = 0$ . Then, the system is equivalent to the independent  $N$  Kitaev chains with different chemical potentials. We assume that there are  $N$  Majorana states. The low energy behavior is described by edge Majorana fermions. The low energy Hamiltonian reads

$$\begin{aligned} H_{\text{eff}} &= -\frac{i|d_y|}{2} \sin \theta \sum_{j=1}^{N-1} (\gamma_j^A \gamma_{j+1}^A - \gamma_j^B \gamma_{j+1}^B) \\ &= -i|d_y| \sin \theta \sum_{j=1}^{N-1} (d_j^\dagger d_{j+1}^\dagger + d_j d_{j+1}), \end{aligned} \quad (27)$$

where  $\gamma_j^A \equiv \gamma_{1,j}^A$  and  $\gamma_j^B \equiv \gamma_{L,j}^B$  are the Majorana fermion operators at the left edge and the right edge of  $j$ -th chain with  $\gamma_{i,j}^{A(B)}$  defined by (10), while  $d_j$  is the ordinary fermion operator constructed from  $\gamma_j^A$  and  $\gamma_j^B$ ,

$$d_j^\dagger = (\gamma_j^A + i\gamma_j^B)/2. \quad (28)$$

This is diagonalized as before and the energy eigenvalues are

$$|d_y| \cos \frac{n\pi}{N+1} \sin \theta \quad (n = 1, \dots, N). \quad (29)$$

By numerically diagonalizing the Hamiltonian (1), we obtain the energy spectrum as a function of  $\theta$  as shown in Fig.7. The low energy levels as a function of the superconducting pairing phase  $\theta$  is in a good agreement with the low-energy theory (29).

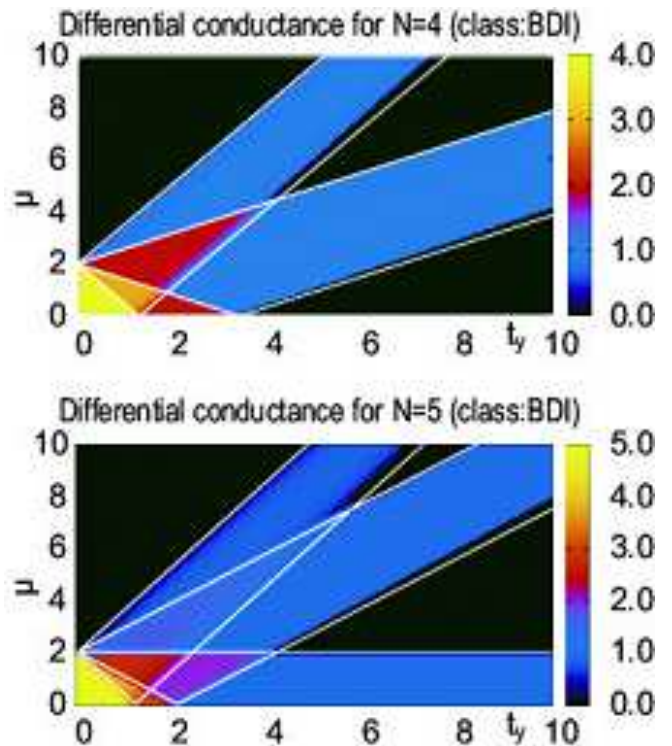


FIG. 8: (Color online) Differential conductance in unit of  $2e^2/h$  with real  $d_y$  when  $N = 4, 5$ . The system belongs to the class BDI. We have taken  $L = 128$ ,  $N = 4$ ,  $t_x = 1.0$ ,  $d_x = 0.5$  and  $d_y = 0.3t_y$ . White lines are topological phase boundaries in Fig.2.

## VI. TRANSPORT PROPERTY

It is well known<sup>20,21</sup> that the local Andreev reflection rate at zero bias is unit in the presence of a Majorana fermion, while the differential conductance is quantized to be  $2e^2/h$ . We calculate the local Andreev reflection (LAR) rate, the crossed Andreev reflection (CAR) rate, the elastic co-tunneling (EC) rate and the normal reflection (NR) rate in our model by means of the recursive Green function method<sup>22–25</sup>. We attach one-dimensional leads to the left and right sides of each chain [Fig.1]. It is known that the scattering matrix  $s$  is related to the retarded Green function  $G^R$  by the Fisher-Lee relation<sup>23</sup>,

$$s_{mn}^{\alpha\beta} = -\delta_{mn}^{\alpha\beta} + i\sqrt{\Gamma_m^\alpha} G^{R\alpha\beta} \sqrt{\Gamma_n^\beta}. \quad (30)$$

Here,  $m$  and  $n$  represent the indices of normal leads;  $\alpha$  and  $\beta$  represent the electron and hole channels;  $s_{mn}^{\alpha\beta}$  is the scattering matrix;  $\Gamma_m^\alpha$  is the relaxation matrix defined by

$$\Gamma_m^\alpha \equiv i(\Sigma_m^{R\alpha} - \Sigma_m^{A\alpha}), \quad (31)$$

with  $\Sigma^R$  and  $\Sigma^A$  being the retarded and advanced self-energies of the lead.

The Green function  $G$  of the total system with the leads is derived by including the self-energies to the Green

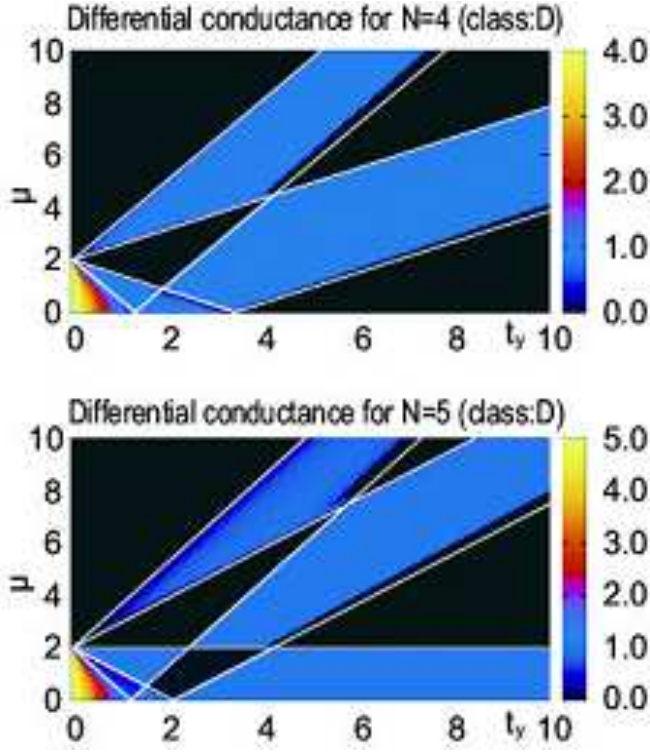


FIG. 9: (Color online) Differential conductance in unit of  $2e^2/h$  with imaginary  $d_y$  when  $N = 4, 5$ . The system belongs to the class D. We have taken  $L = 128, N = 4, t_x = 1.0, d_x = 0.5$  and  $d_y = 0.3it_y$ . White lines are topological phase boundaries in Fig.2.

function  $G_0$  of the system without the leads,

$$G^R(E)^{-1} = G_0^R(E)^{-1} - \Sigma_L^R(E) - \Sigma_R^R(E), \quad (32)$$

where  $\Sigma_L^R$  and  $\Sigma_R^R$  are the self-energies of the left and right leads. In the case of normal leads, the self-energies and thus the relaxation matrix is analytically calculated,

$$\Sigma^R(E) = \tau^\dagger g(E)\tau, \quad (33)$$

with

$$g_{m,n}(E) = \begin{cases} A(k) \left( E_J - i\sqrt{(2t)^2 - E_J^2} \right) & (|E_J| < 2t) \\ A(k) \left( E_J + \sqrt{E_J^2 - (2t)^2} \right) & (E_J < -2t), \\ A(k) \left( E_J - \sqrt{E_J^2 - (2t)^2} \right) & (E_J > 2t) \end{cases}, \quad (34)$$

where  $A(k) = \frac{2}{N+1} \frac{1}{2t^2} \sum_k \sin(kma) \sin(kna)$ ;  $E_J = E + \mu - 2t_y \cos ka$ ,  $t(> 0)$  and  $\mu$  are the hopping and the chemical potential of the leads;  $\tau_{L/R}$  is the coupling matrix of the leads and the system.

From the scattering matrix (30), the transmission and reflection rates can be calculated. There are four processes when the superconducting system is connected by the left and right leads: (i) An electron from the lead L reflects to the lead L as a hole, that corresponds to the

LAR. (ii) An electron from the lead L transmits to the lead R as a hole, that corresponds to the CAR. (iii) An electron from the lead L transmits to the lead R as an electron, that corresponds to the EC. (iv) An electron from the lead L reflects to the lead L as an electron, that corresponds to the NR. The LAR rate  $r_{he}$ , the CAR rate  $t_{he}$ , the EC rate  $t_{ee}$  and the NR rate  $r_{ee}$  are given by

$$r_{he} = |s_{LL}^{he}|^2 = \text{Tr} [\Gamma_L^e G^R \Gamma_L^h G^A], \quad (35)$$

$$t_{he} = |s_{RL}^{he}|^2 = \text{Tr} [\Gamma_L^e G^R \Gamma_R^h G^A], \quad (36)$$

$$t_{ee} = |s_{RL}^{ee}|^2 = \text{Tr} [\Gamma_L^e G^R \Gamma_R^e G^A], \quad (37)$$

$$r_{ee} = |s_{LL}^{ee}|^2 = N + \text{Tr} [\Gamma_L^e G^R \Gamma_L^e G^A] + 2\text{ImTr} [\Gamma_L^e G^R], \quad (38)$$

together with  $r_{he} + t_{he} + t_{ee} + r_{ee} = N$ .

Because the self-energy of the normal lead is known analytically, it is easy to calculate the reflection and transmission rates. We have investigated the cases with real  $d_y$  (class BDI) and with imaginary  $d_y$  (class D). The coupling strength between Majorana fermions at two edges is the order of  $\exp(-L/\xi)$ , where  $\xi$  is the superconducting coherence length. When  $\xi \ll L$ , since there are no overlaps between the MZES localized at the right and left edges, the CAR and EC rates are quite small. Hence the sum of the LAR and NR rates is almost one. On the other hand, when  $\xi > L$ , there are some overlaps between the MZES localized at the right and left edges, and the CAR rate remains finite. The differential conductance is given by

$$G = \frac{e^2}{h} (N - r_{ee} - t_{ee} + r_{he} + t_{he}). \quad (39)$$

The results for the differential conductance  $G$  at zero energy are illustrated in Figs.8 and 9. In both of the classes BDI and D, the figure of the conductance strongly resembles the phase diagrams (Fig.2). The bright regions where the differential conductance is quantized correspond to the topological regions. It means that the LAR rate is one with each MZES. It agrees with the previous study<sup>20,26,27</sup> that the Majorana fermion induces the resonant Andreev reflection.

We also calculated the differential conductance as a function of the superconducting pairing phase  $\theta$  and the energy of injected electron, which we show in Fig.10. The behavior reflects the behavior of the energy spectrum given in Fig.7. Moreover, the differential conductance per mode is quantized to  $2e^2/h$  when  $\theta = 0, \pi$ . This is because of the resonant Andreev reflection induced by Majorana fermions. Furthermore, the peak decays rapidly when the phase is switched on and there are no Majorana fermions.

## VII. CONCLUSION

In conclusion, motivated by a system of InSb nanowires, we have investigated the ladder topological

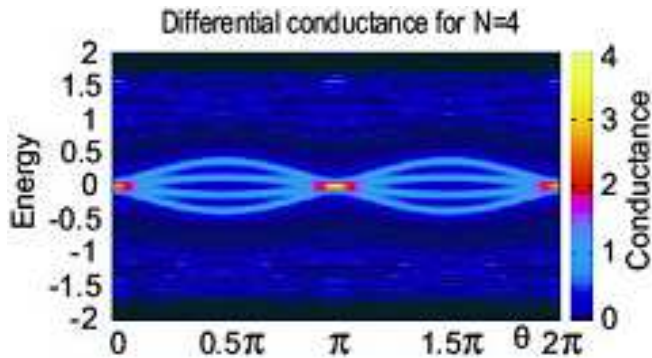


FIG. 10: (Color online) Differential conductance in unit of  $2e^2/h$  as a function of the superconducting pairing phase  $\theta$ . The horizontal axis is  $\theta$  and the vertical axis is the energy. The color map is the differential conductance in unit of  $2e^2/h$ . There are four MZES in the case of  $N = 4$ .

superconductors based on the effective Hamiltonian (1). We have found that the superconducting pairing phase

difference between the  $x$  and  $y$  directions (i.e., the phase of  $d_y/d_x$ ) plays a crucial role to determine the topological class. If the phase is 0 or  $\pi$ , the system belongs to the class BDI with  $n$  MZES ( $n \in \mathbb{Z}$ ); otherwise it belongs to the class D with  $n$  MZES ( $n = 0, 1$ ). The superconducting phase of  $d_y$  might be controlled by applying magnetic field or Josephson current. First, the direction of the magnetic field is important<sup>28,29</sup>. When the magnetic field is along the wires, the system belongs to the class BDI, while the system turns into the class D when the magnetic field parallel to the spin-orbit magnetic field. Second, the phase gradient of the bulk superconductor can be changed by driving supercurrent or by forming the SQUID configuration. The proximity induced pairing in the wires also gets a phase gradient, yielding an imaginary part to  $d_y$ , and the class becomes D. This topological class change will be observed by the Andreev reflection and differential conductance.

This work was supported in part by Grants-in-Aid for Scientific Research from the Ministry of Education, Science, Sports and Culture No. 24224009 and 25400317.

- 
- <sup>1</sup> J. Alicea, Rep. Prog. Phys. **75**, 076501 (2012).
  - <sup>2</sup> C.W.J. Beenakker, Annu. Rev. Con. Mat. Phys. **4**, 113 (2013)
  - <sup>3</sup> L. Fu and C. L. Kane, Phys. Rev. Lett. **100**, 096407 (2008).
  - <sup>4</sup> Y. Oreg, G. Refael and F. von Oppen, Phys. Rev. Lett. **105**, 177002 (2010).
  - <sup>5</sup> R. M. Lutchyn, J. D. Sau, and S. Das Sarma, Phys. Rev. Lett. **105**, 077001 (2010).
  - <sup>6</sup> A. Kitaev, Physics-Uspekhi **44**, 131 (2001).
  - <sup>7</sup> A. C. Potter and P. A. Lee, Phys. Rev. Lett. **105**, 227003 (2010).
  - <sup>8</sup> Y. Niu, S. B. Chung, C.-H. Hsu, I. Mandal, S. Raghu, and S. Chakravarty, Phys. Rev. B, **85**, 035110 (2012)
  - <sup>9</sup> M. -T. Rieder, G. Kells, M. Duckheim, D. Meidan, and P. W. Brouwer, Phys. Rev. B, **86**, 125423 (2012).
  - <sup>10</sup> G. Kells, D. Meidan, and P. W. Brouwer, Phys. Rev. B, **85**, 060507 (2012).
  - <sup>11</sup> D. Asahi and N. Nagaosa, Phys. Rev. B, **86**, 100504(R) (2012).
  - <sup>12</sup> B. Zhou and S.-Q. Shen, Phys. Rev. B, **84**, 054532 (2011).
  - <sup>13</sup> S. R. Manmana, A. M. Essin, R. M. Noack, and V. Gurarie, Phys. Rev. B, **86** 205119 (2012).
  - <sup>14</sup> W. DeGottardi, M. Thakurathi, S. Vishveshwara, and D. Sen, Phys. Rev. B, **88**, 165111 (2013).
  - <sup>15</sup> V. Mourik, K. Zuo, S. M. Frolov, S. R. Plissard, E. P. A. M. Bakkers, and L. P. Kouwenhoven, Science, **336**, 1003 (2012).
  - <sup>16</sup> A. Das, Y. Ronen, Y. Most, Y. Oreg, M. Heiblum, and H. Shtrikman, Nat. Phys. **8**, 887 (2012).
  - <sup>17</sup> M. T. Deng, C. L. Yu, G. Y. Huang, M. Larsson, P. Caroff, and H. Q. Xu, Nano. Lett. **12**, 6414 (2012).
  - <sup>18</sup> L. P. Rokhinson, X. Liu, and J. K. Furdyna, Nat. Phys. **8**, 795 (2012).
  - <sup>19</sup> S. Ryu, A. P Schnyder, A. Furusaki, and A. W. W. Ludwin, New J. Phys. **12**, 065010 (2010).
  - <sup>20</sup> K. T. Law, Patrick A. Lee, and T. K. Ng, Phys. Rev. Lett. **103**, 237001 (2009).
  - <sup>21</sup> L. Fidkowski, J. Alicea, N. H. Lindner, R. M. Lutchyn, and M. P. A. Fisher, Phys. Rev. B, **85**, 245121 (2012).
  - <sup>22</sup> P. A. Lee and D. S. Fisher, Phys. Rev. Lett. **47**, 12 (1981).
  - <sup>23</sup> D. S. Fisher and P. A. Lee, Phys. Rev. B, **23**, 12 (1981).
  - <sup>24</sup> J. J. He, Jiansheng Wu, T.-P. Choy, X.-J. Liu, Y. Tanaka, and K. T. Law, arXiv:1307.2764v3 (2013).
  - <sup>25</sup> J. Liu, F.-C. Zhang, and K. T. Law, Phys. Rev. B, **88**, 064509 (2013).
  - <sup>26</sup> A. Romito, J. Alicea, G. Refael, and F. von Oppen, Phys. Rev. B, **85**, 020502 (2012).
  - <sup>27</sup> K. Flensberg, Phys. Rev. B, **82**, 180516 (2010).
  - <sup>28</sup> S. Tewari and J. D. Sau, Phys. Rev. Lett. **109**, 150408 (2012).
  - <sup>29</sup> S. Tewari, T. D. Stanescu, J. D. Sau, and S. Das Sarma, Phys. Rev. B, **86**, 024504 (2012).